Clarke, M. W., Barbet, A. F., & Pearson, T. W. (1987) *Mol. Immunol. 24*, 707–713.
Cohen, C., & Phillips, G. N. (1971) *Proc. Natl. Acad. Sci. U.S.A. 78*, 5303–5304.
Cohen, C., Reinhardt, B., Parry, D. A. D., Roelants, G. E., Hirsch, W., & Kanwe, B. (1984) *Nature (London) 311*, 169–171.
Crick, F. H. C. (1953) *Acta Crystallogr. 6*, 689–697.
Cross, G. A. M. (1975) *Parasitology 75*, 133–142.
Donelson, J. E., & Rice-Ficht, A. C. (1985) *Microbiol. Rev. 49*, 107–125.
Duvillier, G., Aubert, J. P., Baltz, T., Richet, C., & Degand, P. (1983) *Biochem. Biophys. Res. Commun. 110*, 491–498.
Ferguson, M. A. J., & Cross, G. A. M. (1984) *J. Biol. Chem. 259*, 3011–3015.
Freymann, D. M., Metcalf, P., Turner, M., & Wiley, D. C. (1984) *Nature (London) 311*, 167–169.
Geysen, H. M., Barteling, S. J., & Meloen, R. H. (1985) *Proc. Natl. Acad. Sci. U.S.A. 82*, 178–182.
Gomes, V., Huet-Duvillier, G., Aubert, J. P., Dirat, I., Tetaert, D., Moncany, M. L. J., Richet, C., Vervoort, T., Pays, E., & Degand, P. (1986) *Arch. Biochem. Biophys. 249*, 427–436.
Jahnig, F., Bulow, R., Baltz, T., & Overath, P. (1987) *FEBS Lett. 221*, 37–42.
Johnson, J. G., & Cross, G. A. M. (1979) *Biochem. J. 178*, 689–697.
Lalor, T. M., Kjeldgaard, M., Shimamoto, G. T., Strickler, J. E., Konigsberg, W. H., & Richards, F. F. (1984) *Proc. Natl. Acad. Sci. U.S.A. 81*, 998–1002.
Lanham, S. M., & Godfrey, D. G. (1970) *Exp. Parasitol. 28*, 521–534.
Lepage, R. W. F. (1967) *Trans. R. Soc. Trop. Med. Hyg. 61*, 139–140.
Metcalf, P., Blum, M., Freymann, D., Turner, M., & Wiley, D. C. (1987) *Nature (London) 325*, 84–86.
Miller, E. N., Allan, L. M., & Turner, M. J. (1984a) *Mol. Biochem. Parasitol. 13*, 67–81.
Miller, E. N., Allan, L. M., & Turner, M. J. (1984b) *Mol. Biochem. Parasitol. 13*, 309–322.
Olafson, R. W., Clarke, M. W., Kielland, S., Pearson, T. W., Barbet, A. F., & McGuire, T. C. (1984) *Mol. Biochem. Parasitol. 12*, 287–298.
Pays, E., van Assel, S., Laurent, M., Darville, M., Vervoort, T., van Miervenne, N., & Steinert, M. (1983) *Cell (Cambridge, Mass.) 34*, 371–381.
Provencher, W. W., & Glöckner, J. (1981) *Biochemistry 20*, 33–37.
Rice-Ficht, A. C., Chen, K. K., & Donelson, J. E. (1982) *Nature (London) 298*, 676–679.
Richards, E. G., Teller, D. C., & Schachaman, H. K. (1968) *Biochemistry 7*, 1054–1076.
Strickler, J. E., Binder, D. A., L'Italien, J. J., Shimamoto, G. T., Wait, S. W., Dalheim, L. J., Novotny, J., Radding, J. A., Konigsberg, W. H., Armstrong, M. Y. K., Richards, F. F., & Lalor, T. M. (1987) *Biochemistry 26*, 796–805.
Turner, M. J. (1985) *Ann. Immunol. (Paris) 136C*, 41–49.
Vita, C., Fontana, A., & Chaiken, M. (1985) *Eur. J. Biochem. 151*, 191–196.

Time-Resolved Europium(III) Luminescence Excitation Spectroscopy: Characterization of Calcium-Binding Sites of Calmodulin†

William DeW. Horrocks, Jr.,* and Joel M. Tingey
Department of Chemistry, The Pennsylvania State University, University Park, Pennsylvania 16802
Received July 14, 1987

ABSTRACT: Pulsed-dye laser excitation and lifetime spectroscopy of the $^7F_0 \rightarrow {}^5D_0$ transition of Eu^{3+} reveals details of the binding of this ion to the calcium-binding sites of calmodulin (labeled I–IV, starting at the N-terminus). For 10 μM calmodulin Eu^{3+} binds quantitatively at sites I and II and more weakly at sites III and IV with K_d values of approximately 0.5 μM and 1.0 μM at the latter sites. In D_2O solution the time course of luminescence emission of Eu^{3+}-loaded calmodulin can be separated into three exponential components with lifetimes of 2.50 (sites I and II) and 1.70 and 0.63 ms (sites III and IV). This finding permits the time resolution of the excitation spectrum by determination of the amplitudes of the three components as the excitation wavelength is scanned across the spectral profile in 0.1-nm increments. The amplitudes (intensities at time $t = 0$) are plotted as a function of wavelength and the results fitted to three Lorentzian peaks centered at 579.20, 579.40, and 579.32 nm in order of decreasing lifetimes. In H_2O solution only two exponential luminescence decay components are resolvable with lifetimes of 0.41 and 0.27 ms, corresponding to sites I and II and sites III and IV, respectively. These results indicate that two water molecules are coordinated to the Eu^{3+} ions at sites I and II and at either site III or site IV, with three water molecules at the remaining site. By observation of Förster-type energy transfer in D_2O solutions of calmodulin containing Eu^{3+}/Nd^{3+} energy donor–energy acceptor mixtures, the distances between sites I and II and between sites III and IV were found to be 12.1 ± 0.5 and 11.6 ± 0.8 Å, respectively.

Excitation spectroscopy of the $^7F_0 \rightarrow {}^5D_0$ transition of europium(III) ions bound at calcium ion binding sites in proteins provides a wealth of information regarding the metal ion binding characteristics and structure of calcium-binding proteins (Horrocks & Sudnick, 1979a, 1981). This experiment involves excitation of the $^5D_0$ excited state of Eu^{3+} while a tunable dye laser is scanned in the 578–580-nm region.

† This work was supported by the U.S. Public Health Service through Grant GM23599 from the National Institutes of Health.

0006-2960/88/0427-0413$01.50/0 © 1988 American Chemical Society

Emission of the $^5D_0 \rightarrow {}^7F_2$ transition is monitored at 615 nm. In favorable cases distinct classes of binding site are distinguished by having $^7F_0 \rightarrow {}^5D_0$ excitation peaks at different frequencies. Work in this laboratory (Albin & Horrocks, 1985) has shown that the frequency of the excitation transition correlates with the total formal negative charge on the ligands coordinated to Eu^{3+}. Thus for calcium-binding proteins a measurement of this frequency provides a rough count of the number of negative carboxylate ligands (from Asp or Glu) that are present at the metal ion binding sites. By measuring the excited-state lifetime of Eu^{3+} separately in H_2O and D_2O solutions, it is possible to ascertain the number of water molecules coordinated to the Eu^{3+} ion at a particular binding site (Horrocks & Sudnick, 1979b). Additionally, in situations where calcium-binding sites are within ~15 Å of one another in a protein it is possible to measure distances between such sites by monitoring Förster-type energy transfer between an emissive ion, e.g., Eu^{3+}, and an energy acceptor ion, e.g., Nd^{3+} (Horrocks et al., 1975, 1980).

These techniques have recently been applied by us (Mulqueen et al., 1985) to calmodulin (CaM)[1] [for recent reviews see Manalan and Klee (1984) and Cox et al. (1984)], the object of the present study. Calmodulin, a ubiquitous intracellular protein, functions as a sensor of the calcium concentration transient that occurs upon cell stimulation. CaM binds up to four calcium ions [for recent reviews see Potter et al. (1983), Cox et al. (1984), and Forsén et al. (1986)] in helix–loop–helix domains which occur in pairs at the two globular ends of this dumbbell-shaped molecule (Babu et al., 1985). Starting at the N-terminus, these domains are labeled I–IV. The preponderance of evidence suggests that there are two high-affinity sites for Ca^{2+} (in domains III and IV) and two sets of lower affinity (in domains I and II). On the basis of tyrosine-sensitized Tb^{3+} luminescence (Kilhoffer et al., 1980a,b; Wang et al., 1982, 1984; Mulqueen et al., 1985) and ^{25}Mg nuclear magnetic resonance (Tsai et al., 1987) experiments it appears that sites I and II are the high-affinity sites for Ln^{3+} and Mg^{2+} ions, with sites III and IV having a lower affinity for these ions. It may well be that sites I and II are continuously filled with either Mg^{2+} or Ca^{2+} under physiological conditions and that the triggering action involves Ca^{2+} binding to sites III and IV.

Although the four binding sites are not structurally identical, they are extremely similar, each with either three or four carboxylate moieties as well as peptide carbonyl groups poised to act as ligands to a bound metal ion. Not surprisingly then, these four sites, when simultaneously occupied by Eu^{3+} ions, are not resolved in the frequency domain of the $^7F_0 \rightarrow {}^5D_0$ excitation experiment. As shown in Figure 1, a single peak, apparently composed of several components (individual Eu^{3+} environments have been found to give good Lorentzian–Gaussian peaks), grows in with slight changes in shape and peak position in the course of a titration of apo-CaM with Eu^{3+}.

The present research will demonstrate that while this excitation spectrum is not readily resolvable into individual components in the frequency domain, it can be time-resolved into component peaks corresponding to particular binding sites. By working in D_2O solution and carrying out careful measurements of the time course of luminescence emission, we were able to resolve the observed decays into component exponentials which arise from Eu^{3+} ions occupying different binding sites that have different intrinsic excited-state lifetimes.

[1] Abbreviations: CaM, calmodulin; Ln^{3+}, trivalent lanthanide ion; EDTA, ethylenediaminetetraacetic acid; HEPES, *N*-(2-hydroxyethyl)-piperazine-*N'*-2-ethanesulfonic acid; fwhm, full width at half-maximum.

Materials and Methods

Calmodulin was purified from bovine testicles (Pel-Freeze, Inc.), and the concentration of EDTA in the purified calmodulin was reduced to less than 0.05 equiv by methods described previously (Mulqueen et al., 1985). All calmodulin solutions were buffered at pH 7.0 with 50 mM HEPES and made 0.5 M in KCl to avoid nonspecific Ln^{3+} binding and the resulting precipitation that is observed at lower salt concentrations. The concentration of calmodulin was determined by using a molar absorbancy of $\epsilon_{276} = 3000\ M^{-1}\ cm^{-1}$ in the presence of metal ions and $\epsilon_{276} = 3300\ M^{-1}\ cm^{-1}$ in the absence of metal ions (Wang et al., 1982).

All chemicals were of the highest grade commercially available. Doubly distilled water that had been passed over a Chelex 100 column was used throughout. In order to reduce metal ion contamination, only acid-washed glassware was used. The metal ion solutions were prepared with doubly distilled water from the chloride salts and standardized by a chelometric technique (Fritz et al., 1958).

A Nd:YAG pumped-dye laser pulsed at 10 Hz was used to obtain the excitation spectra and lifetime data. The details of this system are described elsewhere (Tingey, 1987). Luminescence decays during the course of a titration were collected for a set number of laser pulses and corrected for fluctuations in laser power during the course of the experiment. Figure 2, panel A shows a typical luminescence decay curve (10 μM CaM and 3.2 equiv of Eu^{3+} in D_2O solution, 1000 transients summed). The decays were analyzed into a sum of component exponential functions according to a nonlinear regression method developed by Marquardt (1963) which minimizes χ^2, the sum of the squares of differences between observed and calculated quantities. Figure 2, panel B, shows a plot of the weighted residuals of a fit of the data in panel A to a single exponential function. The systematic deviation from the zero line indicates an unacceptable fit. Shown in panel C is the analogous plot for a fit of the data to three exponential functions; it exhibits symmetric deviations from zero, indicative of a good fit. In our analyses, whenever three exponentials were present, the value of at least one of the lifetimes was established from other data and held constant in the Marquardt fitting procedure. The binding curves for the titration data were calculated on the assumption of independent binding sites by Newton's method for nonlinear systems (Feldman et al., 1972).

Results

Figure 1 shows the conventional excitation spectra of the $^7F_0 \rightarrow {}^5D_0$ transition of Eu^{3+} bound to CaM at various metal ion to protein ratios. These spectra were recorded with the laser operating at 10 Hz and by scanning the excitation wavelength at 0.15 nm/min from 578.5 to 580.0 nm. Emitted light was monitored at 615 nm. After each laser flash a 6-μs delay was allowed before photon counting commenced; photon collection continued for 12 ms following each laser pulse. The total number of photons thus recorded for fifty consecutive pulses was accumulated in each channel of the signal averager as the spectrum was scanned. Recorded in this manner, the intensity of an excitation spectrum is proportional to the total number of photons emitted and does not discriminate among long- and short-lived Eu^{3+} species, except insofar as their quantum yields and relative absorptivities at the excitation wavelength are different. The shape of the excitation signal changes discernibly during the course of the titration, and while clearly not a single Lorentzian or Gaussian peak at any point,

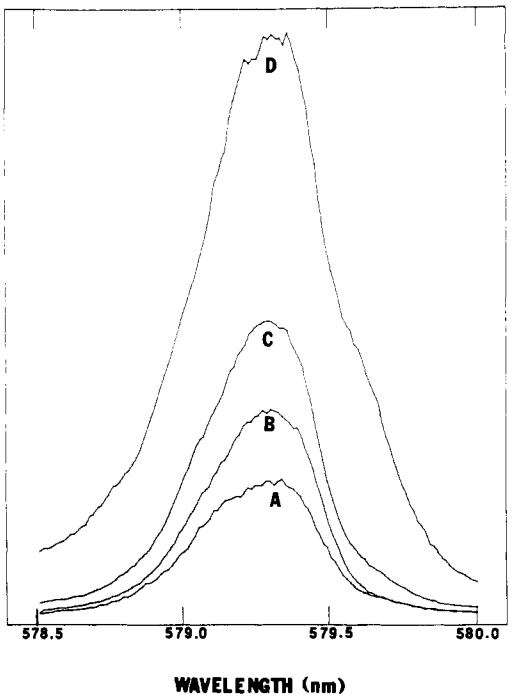

FIGURE 1: $^7F_0 \rightarrow {}^5D_0$ excitation spectra (λ_{em} = 615 nm) of Eu^{3+} bound to calmodulin (10 μM) at Eu^{3+}/calmodulin ratios of (A) 1.00, (B) 1.50, (C) 2.00, and (D) 4.75.

it is not easily resolved into the individual components that might be expected for the four calcium-binding sites in CaM.

Although the excitation spectrum of the Eu^{3+} ions occupying the several calcium-binding sites in CaM is not readily resolvable in the frequency domain, it turns out that the time course of luminescence from fully Eu^{3+} loaded CaM in D_2O solution can be resolved into three component exponential decays characterized by excited-state lifetimes of 2.50, 1.70, and 0.63 ms. These values represent the intrinsic lifetimes of Eu^{3+} in the various binding environments in the absence of coordinated H_2O, in which solvent only two, much shorter lifetimes of 0.41 and 0.27 ms are resolved from the luminescence decay. The finding that individual classes of site exhibit significantly different intrinsic lifetimes in a D_2O environment provides us with the ability to time resolve the excitation spectra into individual components corresponding to the various sites.

Figure 3 shows the results of such a resolution. The time courses of luminescence emission were recorded at 0.1-nm intervals from 578.5 to 579.9 nm. In the central region (578.5–579.6 nm) 1000 emissions were recorded and averaged at each wavelength, while in the wings up to 5000 emissions were averaged in order to achieve a good signal to noise ratio. These experiments were carried out on 10 μM CaM samples containing 2 or 4 equiv of added Eu^{3+}. Data from the former samples served to establish the lifetime (2.38 ms) of Eu^{3+} in the first sites occupied (sites I and II). With this lifetime held constant, the decay curves in the 579–580-nm region with 4 equiv of Eu^{3+} were analyzed for the two shorter lived components and their amplitudes (intensities at time t = 0). The data from CaM with 4 equiv of Eu^{3+} in the 578.5–579.0-nm region were observed to contain a nonneglible contribution from the Eu^{3+} aqua ion (λ_{max} = 578.8 nm, τ = 2.43 ms), and this portion of the spectrum was analyzed with the aqua ion contribution, estimated from the difference between the data at 2 and 4 equiv, subtracted out. The lifetimes for the two shorter lived components (Eu^{3+} in sites III and IV) were found to be 1.80 and 0.70 ms in this analysis. The small differences between the lifetimes quoted above and the pure D_2O results

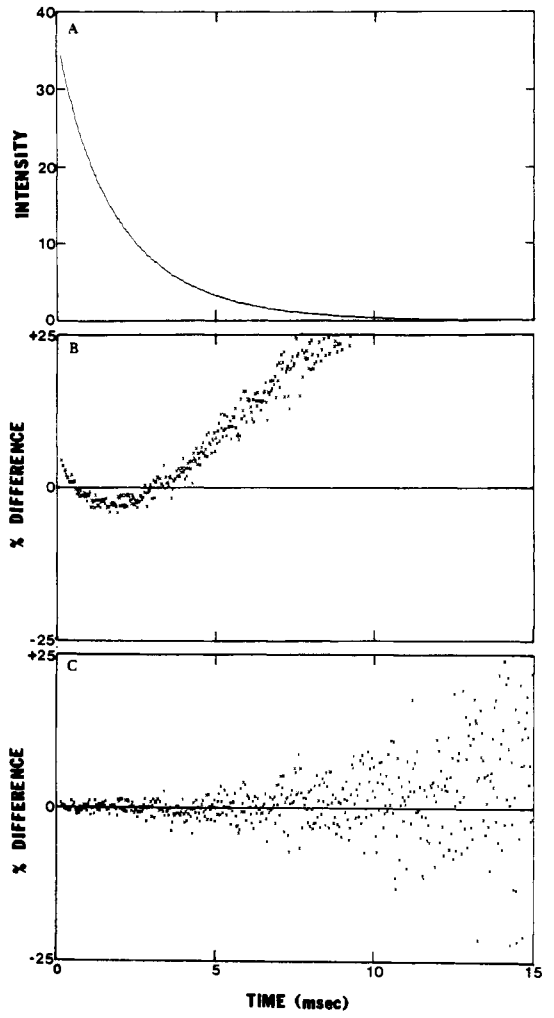

FIGURE 2: Panel A: Luminescence decay curve (λ_{ex} = 579.3 nm, λ_{em} = 615 nm) of Eu^{3+} in calmodulin (10 μM CaM and 3.2 equiv of Eu^{3+} in D_2O solution, 1000 transients summed). Panel B: Weighted residual plot of fit of data of panel A to a single exponential function. Panel C: Weighted residual plot of fit of data of panel A to sum of three exponential functions.

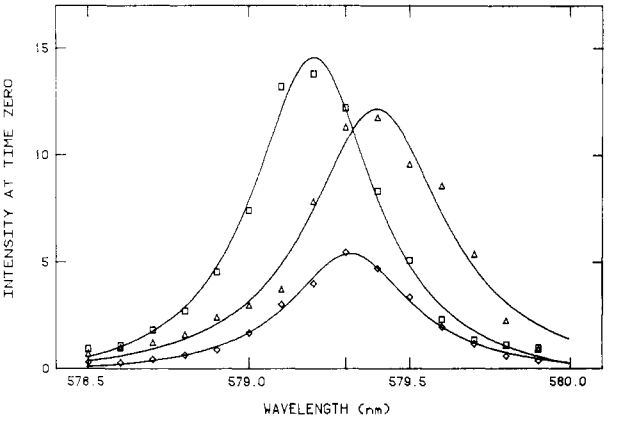

FIGURE 3: Time-resolved excitation spectrum (λ_{em} = 615 nm) of calmodulin (10 μM in D_2O solution, pH 7.0) containing 4.0 equiv of Eu^{3+}: (□) τ = 2.38 ms; (◇) τ = 0.70 ms; (△) τ = 1.80 ms.

arise from the fact that H_2O was not as rigorously excluded from this system. The same comment applies to the analysis of the titration data described later. Plotted in Figure 3 are the amplitudes of the three resolved lifetime components as a function of wavelength. Lorentzian line shapes have been least squares fitted to the data points. These curves represent the excitation spectral peaks that would be obtained were the three classes of site separately occupied by Eu^{3+} ions. The

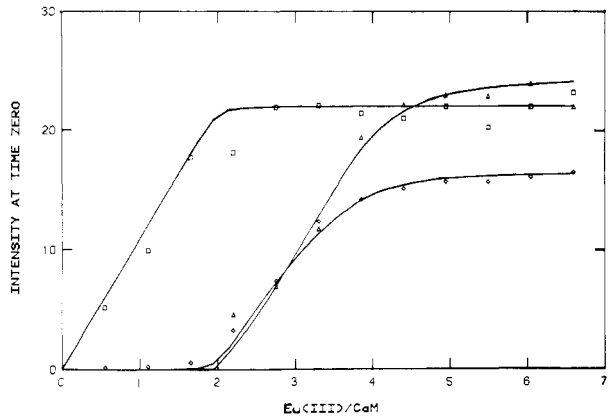

FIGURE 4: Amplitudes of the three component exponential functions of Eu^{3+} luminescence decay curves (λ_{ex} = 579.3 nm, λ_{em} = 615 nm) as a function of equivalents of added Eu^{3+} as this ion is titrated into apocalmodulin (10 μM in D_2O solution at pH 7.0): (□) τ = 2.40 ms; (◇) τ = 0.63 ms; (△) τ = 1.70 ms.

quantity plotted corresponds to the emission intensity observed at the instant of excitation (t = 0). The height of each curve is proportional to the product of the number of Eu^{3+} ions excited by the laser at a particular wavelength and the rate constant for radiative emission k_{rad} of Eu^{3+} in a particular site. Unlike excitation spectra recorded in the usual manner (Figure 1), the intensities of time-resolved peaks are independent of the quantum yield of Eu^{3+} in a particular site. The Lorentzian curves correspond to three classes of binding site. They peak at slightly different wavelengths, 579.20, 579.32, and 579.40 nm, with peak width (fwhm) values of 0.46, 0.47, and 0.52 nm for the environments having lifetimes of 2.38, 0.70, and 1.80 ms, respectively.

Titration of Apo-CaM with Eu^{3+} Monitored by Time-Resolved Luminescence. At 579.3 nm (the extra hatch mark in Figure 3) all three classes of Eu^{3+} contribute substantially to the luminescence emission. This wavelength was chosen to monitor the filling of the metal ion binding sites as apo-CaM is titrated with Eu^{3+}. The amplitudes derived from the multiexponential analysis of the decay curves at each Eu^{3+} addition are plotted in Figure 4 as a function of the ratio of added Eu^{3+} to CaM. Up until 2 equiv of Eu^{3+} are added, the luminescence decay is described by a single exponential with a lifetime of 2.40 ms. These data are consistent with the quantitative initial filling of two tight sites with indistinguishable Eu^{3+} excited-state lifetimes. (The isotopic composition of the solution used for this titration differs slightly from that used for the time resolution of the excitation spectra; hence the lifetimes are slightly different.) Beyond this amount of added Eu^{3+} the decay is described by a sum of three exponentials. In order to determine the additional two lifetimes accurately, the decay data for 2.2 equiv of added Eu^{3+} were subtracted from all subsequent decays and the resulting curves were analyzed for the two additional lifetimes, yielding 1.70 and 0.63 ms. After the three lifetimes had been established with certainty, these values were held constant and the full decay curves were analyzed for the individual amplitudes, which are plotted in Figure 4. Following the filling of the two tight sites, Eu^{3+} goes to two weaker sites which compete with one another. The solid curves through the points in Figure 4 were calculated for assumed dissociation constants of 1×10^{-9} M for the tight sites and 5×10^{-7} M (τ = 0.63 ms) and 1×10^{-6} M (τ = 1.70 ms) for the weaker sites.

Determination of the Number of Water Molecules Coordinated to Eu^{3+} at Each Site. Our ability to resolve temporally three classes of Eu^{3+} bound to CaM allows us to interrogate these individual sites regarding the number of water molecules coordinated at each site. Earlier work in this laboratory (Horrocks & Sudnick, 1979a,b) has shown that the measurement of lifetimes separately in H_2O and D_2O solution provides a measure of the number of Eu^{3+}-coordinated water molecules q according to

$$q = 1.05(\tau_{H_2O}^{-1} - \tau_{D_2O}^{-1}) \quad (1)$$

As described above, the sites in CaM give rise to three different lifetimes in D_2O as indicated in Table I. In H_2O solution with up to 2 equiv of Eu^{3+} only a single exponential decay (τ = 0.41 ms) is observed; however, when 4 equiv of Eu^{3+} are present, the decay curve is resolvable into two exponentials, the second of which has a τ value of 0.27 ms. The ratio of the amplitudes of the short-lived component to that of the long-lived exponential is ~1.3, in good agreement with the expected ratio based on the resolved excitation curves of Figure 4 if the shorter τ represents both of the weaker sites. These data are set out in Table I along with the derived number of coordinated water molecules. The two tight sites (I and II) both involve two coordinated water molecules while one of the weaker sites (III or IV) has two coordinated water molecules and the other has three. The standard deviations associated with each of the lifetime measurements are given in Table I, but the major source of uncertainty arises from the empirical fit to the data used to determine eq 1 (Horrocks & Sudnick, 1979b).

Table I: Data for Determination of the Number of Water Molecules, q, Coordinated to Eu^{3+}

	D_2O		H_2O	
sites	τ (ms)	τ^{-1} (ms^{-1})	τ^{-1} (ms^{-1})	q
I and II	2.50 ± 0.10	0.40 ± 0.02	2.43 ± 0.05	2.1 ± 0.5
III or IV	1.70 ± 0.10	0.59 ± 0.03	3.70 ± 0.40	3.3 ± 0.5
III or IV	0.63 ± 0.05	1.59 ± 0.10	3.70 ± 0.40	2.2 ± 0.5

Table II: Parameters of Förster-Type Energy Transfer and Distance Measurements[a]

sites	τ_0 (ms)	τ_{Nd} (ms)	E^b	ϕ	R_0 (Å)[c]	r (Å)[d]
I and II	2.24 ± 0.02	1.45 ± 0.02	0.352	0.70	11.0	12.1 ± 0.5
III or IV	1.60 ± 0.02	1.14 ± 0.02	0.287	0.39	10.0	11.6 ± 0.8
III or IV	0.63 ± 0.02	0.50 ± 0.02	0.206	0.25	9.3	11.6 ± 0.8

[a] See text for definition of symbols. [b] $E = 1 - (\tau_{Nd}/\tau_0)$. [c] $R_0^6 = (8.78 \times 10^{-25})\kappa^2\phi n^{-4}J$. [d] $r = R_0[(1 - E)/E]^{1/6}$.

Distance Measurements from Förster-Type Nonradiative Energy Transfer. In an earlier study we made use of nonradiative energy transfer between excited Eu^{3+} ions and Nd^{3+} ions in sites I and II of CaM. Using the same protocol, wherein the energy-transfer efficiency E is measured by means of the effect on the excited-state lifetime of Eu^{3+} of a nearby Nd^{3+} ion, we now report the distance between sites III and IV. Owing to our ability to time resolve signals from the Eu^{3+} ions in sites III and IV, we are now able to measure the distance between these two sites. The pairs of sites (I and II vs III and IV) are too far separated by the long central α-helical domain of CaM to exhibit measurable energy transfer between them. Förster theory is well established, and the requisite equations and parameters employed are given in Table II along with the Eu^{3+} lifetimes in the absence (τ_0) and presence (τ_{Nd}) of energy transfer and the derived energy-transfer efficiencies. The parameters that go into the determination of R_0, the critical distance for 50% energy transfer, are κ^2, the orientation factor; ϕ, the quantum yield of the donor in the absence of acceptor; n, the refractive index; and J, the spectral overlap integral. For reasons discussed in our earlier

papers (Mulqueen et al., 1985; Rhee et al., 1981) n was taken as 1.35, κ^2 was taken as the isotropic limit, $^2/_3$, and J was experimentally determined from the corrected emission spectrum of Eu^{3+} in CaM and the absorption spectrum of Nd^{3+} bound to the two tight sites ($J = 1.40 \times 10^{-17}$ cm^6 mol^{-1} on a per mole of Nd^{3+} basis). For the analysis of energy transfer from the $^5D_0$ excited state of Eu^{3+} the quantum yield of this level is required for each Eu^{3+} site that acts as an energy donor. Because of the extremely weak and narrow absorption profile of the $^7F_0 \rightarrow {}^5D_0$ transition, the quantum yield of this level is not known with certainty, even in model systems. The quantum yield of the Eu^{3+} aqua ion in D_2O solution has been given as 0.78 (Stein & Wurzberg, 1975), but this value is based on a standard of uncertain reliability (Dawson & Kropp, 1965). Thus we are forced to assume reasonable values for this quantity and to assess the uncertainty imposed upon the derived distances. Assuming values of ϕ from 1.0 to 0.6 gave a range of R_0 values from 11.6 to 10.8 Å and, on the basis of the measured energy-transfer efficiency, distances r between sites I and II from 12.9 to 12.0 Å. For the present purposes we will assume $\phi = 0.70$ for Eu^{3+} in sites I and II ($\tau = 2.24$ ms). The problem remains, then, to estimate the quantum yields corresponding to the sites with τ values of 1.60 and 0.63 ms. These lifetimes, especially the latter, are quite short for D_2O solutions, a circumstance that could arise if the radiative rate constant for emission of photons, k_{rad}, were particularly large or, alternatively, if the nonradiative deexcitation rate constant, k_{nonrad}, of ions in these sites were particularly enhanced.

If one assumes that k_{rad} for Eu^{3+} in all four sites of CaM is the same, then any differences in the observed lifetimes are due to nonradiative processes and their relative quantum yields are just the ratios of the observed lifetimes. With the assumption that $\phi = 0.70$ for the $\tau = 2.24$ ms sites, this leads to quantum yields of 0.50 for the $\tau = 1.60$ ms site and 0.20 for the $\tau = 0.63$ ms site. These latter values when used in the R_0 calculation lead to distances of 12.1 and 11.1 Å, respectively, between sites III and IV. On the other hand, differences in k_{rad} might account entirely for the differences in observed lifetimes. It can be shown that k_{rad}^2 values are likely to be portional to the areas under the individual time-resolved excitation spectral peaks. The arguments for this are based on the Einstein relationship for a two-level system and are set out elsewhere (Tingey, 1987). Under this assumption, and again assuming $\phi = 0.70$ for the tight sites, one obtains $\phi = 0.65$ and 0.15 for the $\tau = 1.60$ and 0.63 ms sites, respectively. These numbers lead to measured distances of 12.6 and 10.6 Å, respectively. Since the distance from site III to site IV is the same as the reverse direction, the above nonrigorous methods of estimation of quantum yields are imperfect and a satisfactory compromise must be sought. In Table II are listed quantum yield values and derived distances that represent a realistic and consistent compromise among the above-described methods. The uncertainties quoted were obtained according to the considerations outlined above.

Discussion

Although the $^7F_0 \rightarrow {}^5D_0$ transition between nondegenerate levels can in principle distinguish among nonequivalent Eu^{3+} environments, the total frequency difference for 36 systems ranging in total charge on the ligands from 0 to −6 was only 49 cm^{-1} out of ~17 250 cm^{-1}. It is not surprising, then, that separate resolvable peaks do not always occur for different Eu^{3+} environments, particularly in protein systems where Eu^{3+} ions in individual binding sites usually have peak widths (fwhm) of ~15 cm^{-1}. This is the case for the four calcium-binding sites of CaM as seen in Figure 1, where individual components due to the occupancy of different sites are not readily discerned as Eu^{3+} is titrated into apo-CaM.

In the technique introduced here, use is made of the fact that Eu^{3+} ions in different environments will generally not have identical excited-state lifetimes, τ. The reciprocal of an observed lifetime, τ^{-1}, is the sum of the rate constant for radiative, k_{rad}, and nonradiative, k_{nonrad}, deexcitation. The radiative rate constant, k_{rad}, is a function only the electronic structure and will depend upon the ligand field sensed by the Eu^{3+} ion but is independent of isotopic environment, e.g., replacement of H_2O by D_2O. The nonradiative rate constant, k_{nonrad}, is also environmentally sensitive and, in particular, increases by about 0.95 ms^{-1} per coordinated water molecule when compared with the result in D_2O. This effect arises from a nonradiative transfer of electronic energy to the OH vibrational manifold that is much less efficient in the case of OD oscillators and has been exploited by us in the measurement of the number of water molecules coordinated to Eu^{3+} in a variety of protein environments (Horrocks & Sudnick, 1979b). While in some cases where Eu^{3+} environments differ significantly in the number of coordinated water molecules it may be easier to resolve an observed luminescence decay into its exponential components in H_2O, in other cases, including the present one, it is advantageous to work in D_2O solution where k_{nonrad} is a smaller fraction of τ^{-1}. For CaM in D_2O solution we are able to resolve three τ^{-1} values, 0.40, 0.59, and 1.59 ms^{-1}, while in H_2O solution only two components, 2.43 and 3.70 ms^{-1}, are found. Whenever it is possible to resolve a luminescence decay into individual components, it should then be possible to achieve a time resolution of the corresponding excitation spectrum. This is done by carefully analyzing the decay traces into the amplitudes (intensities at time $t = 0$) of the component exponentials at a series of excitation wavelengths across the profile of the spectrum. This has been done for CaM containing 4 equiv of added Eu^{3+} as shown in Figure 3, where the individual amplitudes are plotted as a function of excitation wavelength and fitted to Lorentzian curves.

This time-resolved excitation spectrum is best understood when considered in conjunction with the titration data of Figure 4 where the individual amplitudes measured at 579.3 nm are plotted against the number of equivalents of added Eu^{3+}. It is apparent that the peak corresponding to the longest lived component arises from the Eu^{3+} ions binding to sites I and II. This order of binding for Ln^{3+} ions has been established in several tyrosine-sensitized Tb^{3+} luminescence studies (Kilhoffer et al., 1980a,b; Wang et al., 1982; Mulqueen et al., 1985), although there are two reports (Wallace et al., 1982; Valentini & Wright, 1985) in disagreement with this. Recently, it has been shown (Tsai et al., 1987) that sites I and II are the tighter sites for Mg^{2+} ion binding and may well be continuously occupied by this ion under physiological concentrations of Mg^{2+} and Ca^{2+}. In this sense the two tight Ln^{3+} sites may be "Ca–Mg" structural sites in CaM, and the principal triggering action may arise from Ca^{2+} binding to sites III and IV, which are the weaker sites for Ln^{3+} ions. The excitation peaks corresponding to Eu^{3+} in sites III and IV occur at slightly higher wavelengths. The correlation between net ligand negative charge and frequency of the $^7F_0 \rightarrow {}^5D_0$ transition presented earlier (Albin & Horrocks, 1985) would suggest that sites III and IV have on average a slightly more negative environment, although data on the amino acid sequence suggests three coordinated carboxylate groups at sites I, III, and IV, and four at site II. The empirical correlation did not, however, involve any bidentate carboxylate moieties,

a type frequently found in calcium-binding loops in proteins.

When comparing time-resolved excitation peaks (Figure 3) or amplitude components at a particular wavelength (Figure 4), it is important to be aware of the quantities upon which they depend. The amplitude of a component exponential of a decay at a particular wavelength is proportional to the number of Eu^{3+} ions excited at that particular wavelength by the laser and the radiative rate constant. Nonradiative processes do not affect this quantity. For a given laser pulse intensity, the amplitude will be proportional to the concentration of ground-state Eu^{3+} ions and their absorptivity at that wavelength. Thus the relationship between peak height or area and the ground-state concentration of Eu^{3+} in a particular site is not a simple one. This fact accounts for the finding that for 579.3-nm excitation the final intensity (Figure 4) generated by two Eu^{3+} ions in sites I and II (τ = 2.4 ms) is slightly less than that for the single Eu^{3+} with τ = 1.7 ms.

The site with the shortest lifetime clearly involves an unusually large nonradiative rate process. Whether this is related to the observed quenching (Kilhoffer et al., 1981) of tyrosine-138 in domain IV is not known. Further work is needed to answer this question and to make a definitive assignment of the excitation peaks with the shorter lifetimes to sites III or IV.

The ability to distinguish among these sites on a temporal basis allows us to determine the number of water molecules coordinated to the Eu^{3+} ions at each site. The results, given in Table I, show that two water molecules are involved at the two tight sites (I and II) and at one of the weaker sites. It is perhaps significant that the site (τ = 1.7 ms) fit by the largest dissociation constant (K_d = 1 μM) involves the greatest number of coordinated water molecules (three), perhaps implying weaker ligation of this site by the protein. It should be remembered that Eu^{3+} with its higher formal charge is a surrogate for Ca^{2+} and will not behave identically with Ca^{2+} in all circumstances. Its utility as a probe of Ca^{2+}-binding sites will be enhanced as more metal ion binding sites are examined under high-resolution by X-ray methods, particularly if comparative Ln^{3+}–Ca^{2+} studies become available.

In our earlier paper (Mulqueen et al., 1985) we reported, prior to the appearance of the X-ray structure (Babu et al., 1985) that confirmed our result, the measurement of the distance between sites I and II of CaM. With the present time-resolution methods in hand, we are now able to measure the distance between the two weaker sites for Ln^{3+} ions, sites III and IV. Since we are able to distinguish between energy-donor Eu^{3+} ions in sites III and IV with a Nd^{3+} in the remaining sites, we are, in effect, able to measure this distance twice. Due to our lack of knowledge of and inability to measure quantum yields for the $^5D_0$ state of Eu^{3+} in protein environments, we must rely on certain assumptions to arrive at a final answer. As indicated under Results, neither the assumption that k_{rad} values were the same for all sites nor the assumption that they were proportional to the square roots of the areas under the time-resolved excitation spectral curves leads to a consistent result (same distance in both directions). Table II gives ϕ values that represent a realistic compromise. While this process leads to the fairly large uncertainties quoted, the results are entirely consistent with the known details of the crystal structure. The distances between sites I and II and between sites III and IV are identical to within our experimental error, but our data suggest that the latter pair are slightly nearer one another than the former. Our results show unambiguously that the first two sites filled are in proximity to one another, as are the third and fourth sites. This finding eliminates the possibility that Ln^{3+} binding to CaM occurs in alternative sequences as suggested by others (Wallace et al., 1982; Valentini & Wright, 1985). Due to the much larger separations, we do not expect to observe energy transfer between ions in domains II and III and ions in domains III and IV. Work is in progress on a method that will allow us to measure directly Eu^{3+} quantum yields in proteins and thus eliminate this source of uncertainty in distance measurements.

Conclusions. The ability to time resolve $^7F_0 \rightarrow {}^5D_0$ excitation spectra of Eu^{3+} adds a new dimension to the use of this ion as a probe of calcium-binding proteins. Even in cases where the normal $^7F_0 \rightarrow {}^5D_0$ excitation spectrum is ill resolved in the frequency domain it is possible to interrogate and characterize distinct classes of binding site according to the methods introduced here. One is now able to follow the sequential or simultaneous binding of Eu^{3+} to different binding sites, to obtain a count of the number of coordinated water molecules at each site, and to measure interion distances, which was not possible heretofore. The present results constitute a fairly complete picture of the binding of Eu^{3+} to CaM. These methods are being applied to the study of the interaction of CaM with its target molecules.

ACKNOWLEDGMENTS

We thank Dr. Patrick J. Breen, Charles McNemar, and Gregory K. Farber for writing portions of the computer code used in this study.

Registry No. Eu, 7440-53-1; Ca, 7440-70-2; H_2O, 7732-18-5.

REFERENCES

Albin, M., & Horrocks, W. DeW., Jr. (1985) *Inorg. Chem. 24*, 895–900.

Babu, Y. S., Sack, J. S., Greenbough, T. J., Bugg, C. E., Mans, A. R., & Cook, W. J. (1985) *Nature (London) 315*, 37–40.

Cox, J. A., Comte, M., Malone, A., Burger, D., & Stein, E. A. (1984) *Met. Ions Biol. Syst. 17*, 215–273.

Dawson, W. R., & Kropp, J. L. (1965) *J. Opt. Soc. Am. 55*, 822–828.

Feldman, H., Rodbard, D., & Levine, D. (1972) *Anal. Biochem. 45*, 530–556.

Forsén, S., Vogel, H. J., & Drakenberg, T. (1986) in *Calcium and Cell Function* (Cheung, W. Y., Ed.) Vol. 6, pp 113–157, Academic, New York.

Fritz, J. S., Oliver, R. T., & Pietrzyk, K. J. (1958) *Anal. Chem. 30*, 1111–1114.

Horrocks, W. DeW., Jr., & Sudnick, D. R. (1979a) *Science (Washington, D.C.) 206*, 1194–1196.

Horrocks, W. DeW., Jr., & Sudnick, D. R. (1979b) *J. Am. Chem. Soc. 101*, 334–340.

Horrocks, W. DeW., Jr., & Sudnick, D. R. (1981) *Acc. Chem. Res. 14*, 384–392.

Horrocks, W. DeW., Jr., Holmquist, B., & Vallee, B. L. (1975) *Proc. Natl. Acad. Sci. U.S.A. 72*, 4764–4768.

Horrocks, W. DeW., Jr., Rhee, M.-J., Snyder, A. P., & Sudnick, D. R. (1980) *J. Am. Chem. Soc. 102*, 3650–3652.

Kilhoffer, M. C., Demaille, J. G., & Gerard, D. (1980a) *FEBS Lett. 116*, 269–272.

Kilhoffer, M. C., Gerard, D., & Demaille, J. G. (1980b) *FEBS Lett. 120*, 99–103.

Kilhoffer, M. C., Demaille, J. G., & Gerard, D. (1981) *Biochemistry 20*, 4407–4414.

Manalan, A. S., & Klee, C. B. (1984) *Adv. Cyclic Nucleotide Protein Phosphorylation Res. 18*, 227–278.

Marquardt, D. W. (1963) *J. Soc. Ind. Appl. Math. 11*, 431–441.

Mulqueen, P., Tingey, J. M., & Horrocks, W. DeW., Jr.

(1985) *Biochemistry 24*, 6639–6645.
Potter, J. D., Strang-Brown, P., Walker, P. L., & Iida, S. (1983) *Methods Enzymol. 102*, 135–143.
Rhee, M.-J., Sudnick, D. R., Arkle, V. K., & Horrocks, W. DeW., Jr. (1981) *Biochemistry 20*, 3328–3334.
Stein, G., & Würzberg, E. (1975) *J. Chem. Phys. 62*, 208–213.
Tingey, J. M. (1987) Ph.D. Thesis, The Pennsylvania State University, University Park, PA.
Tsai, M.-D., Drakenberg, T., Thulin, E., & Forsén, S. (1987) *Biochemistry 26*, 3635–3643.
Valentini, M. A., & Wright, J. C. (1985) *Anal. Biochem. 150*, 47–57.
Wallace, R. W., Tallant, E. A., Dockter, M. E., & Cheung, W. Y. (1982) *J. Biol. Chem. 257*, 1845–1854.
Wang, C.-L. A., Aquaron, R. R., Leavis, P. C., & Gergely, J. (1982) *Eur. J. Biochem. 124*, 7–12.
Wang, C.-L. A., Leavis, P. C., & Gergely, J. (1984) *Biochemistry 23*, 6410–6415.

Fluorescence Anisotropy Decay Demonstrates Calcium-Dependent Shape Changes in Photo-Cross-Linked Calmodulin†

Enoch W. Small* and Sonia R. Anderson
Department of Biochemistry and Biophysics, Oregon State University, Corvallis, Oregon 97331
Received June 2, 1987; Revised Manuscript Received August 18, 1987

ABSTRACT: We report dynamic fluorescence anisotropy measurements on the purified dityrosine derivative of calmodulin which was generated during UV irradiation of Ca^{2+}-containing solutions of bovine brain calmodulin [Malencik, D. A., & Anderson, S. R. (1987) *Biochemistry 26*, 695]. Measurements were made by using a high repetition rate picosecond laser source combined with a microchannel plate photomultiplier. This permits the collection of very low noise anisotropy curves with essentially no convolution artifact. Measured anisotropies at high calcium concentrations are monoexponential, and at 20 °C, we recover a correlation time of 9.9 ns. When the temperature is varied from 4.8 to 31.8 °C, the recovered correlation time is proportional to the viscosity and inversely proportional to the absolute temperature, behavior expected for the rotational diffusion of a macromolecule whose conformation is independent of the temperature. The correlation time is compared to the theory describing the rotational diffusion of a dumbbell. At high calcium concentrations, the cross-linked calmodulin is elongated and has a length equal or nearly equal to that predicted by X-ray crystallographic results. In the absence of calcium, the molecule becomes highly compact and exhibits significant segmental motion. Intermediate calcium ion concentrations result in an intermediate degree of elongation and segmental motion. A small increase in the measured rotational correlation time of calmodulin upon the binding of melittin and mastoparan indicates that these peptides cause no major changes in the elongation of the molecule. When the cross-linked calmodulin is bound to troponin I, the complex rotates as a unit with a single rotational correlation time of 22 ns.

Calmodulin is a small acidic protein with a molecular weight of 16 700. In eukaryotic cells, it is the primary mediator of calcium control for a number of metabolic processes. For example, it binds and activates cyclic nucleotide phosphodiesterase (Cheung, 1967), adenylate cyclase (Cheung et al., 1975; Brostrom et al., 1975), and myosin light chain kinase [cf. Perry et al. (1984)]. It also interacts with a number of basic small peptides which compete with the enzymes in the in vitro binding of calmodulin [cf. Anderson and Malencik (1986, 1987)]. Since these associations are strongly calcium dependent, the binding of calcium by calmodulin apparently stabilizes one or more conformations which are conducive to the binding of specific proteins and peptides.

X-ray crystallographic studies of the calcium–calmodulin complex performed at 3.0-Å resolution have revealed a dumbbell-shaped molecule containing two lobes connected by an eight-turn α-helix (Babu et al., 1985). The total length of the molecule is about 65 Å. Each lobe has the approximate dimensions of 25 × 20 × 20 Å and binds two calcium ions through helix–loop–helix domains similar to those found in other calcium-binding proteins. Although the three-dimensional structure of calcium-free calmodulin is still unknown, a number of physical methods have demonstrated conformational changes in calmodulin upon the binding of calcium. These include circular dichroism (Klee, 1977; Wolff et al., 1977; Crouch & Klee, 1980; Hennessey et al., 1987), nuclear magnetic resonance [Seamon, 1980; cf. review by Forsén et al. (1986)], fluorescence (Kilhoffer et al., 1981; Lambooy et al., 1982), and ultraviolet difference spectroscopy (Klee, 1977; Crouch & Klee, 1980). The results obtained with these techniques deal with the microscopic environments of particular chromophores rather than with the overall hydrodynamic properties of the calmodulin molecule. Consequently, they give incomplete information on many of the distinctive structural perturbations initiated by Ca^{2+} binding. For example, circular dichroism—which examines the secondary structure of proteins—reveals little difference between calmodulin folded in potassium chloride in the absence of calcium and calcium-saturated calmodulin (Hennessey et al., 1987). The rotational diffusion studies reported here, on the other hand, are highly

† The work of E.W.S. was supported by NIH Grant GM25663 and by a grant from the Medical Research Foundation of Oregon and that of S.R.A. by grants from the Muscular Dystrophy Association and the National Institutes of Health (DK13912 and NIEHS ES-00210, respectively).

0006-2960/88/0427-0419$01.50/0 © 1988 American Chemical Society